Macrocycle and Substituent Vibrational Modes of Nonplanar Nickel(II) Octaethyltetraphenylporphyrin from Its Resonance Raman, Near-Infrared-Excited FT Raman, and m-IR Spectra and De...

ARTICLE *in* THE JOURNAL OF PHYSICAL CHEMISTRY · APRIL 1993

Impact Factor: 2.78 · DOI: 10.1021/j100117a012 · Source: OAI

Macrocycle and Substituent Vibrational Modes of Nonplanar Nickel(II) Octaethyltetraphenylporphyrin from Its Resonance Raman, Near-Infrared-Excited FT Raman, and FT-IR Spectra and Deuterium Isotope Shifts

Andreas Stichternath,[†] Reinhard Schweitzer-Stenner,*[,†] Wolfgang Dreybrodt,[†] Ronald S. W. Mak,[‡] Xiao-yuan Li,*[,‡] Laurie D. Sparks,[§] John A. Shelnutt,*[,§] Craig J. Medforth,[∥] and Kevin M. Smith[∥]

Institute of Experimental Physics, University of Bremen, 2800 Bremen 33, Germany, Department of Chemistry, Hong Kong University of Science and Technology, Hong Kong, Fuel Science Department 6211, Sandia National Laboratories, Albuquerque, New Mexico 87185, and Department of Chemistry, University of New Mexico, Albuquerque, New Mexico 87131, and Department of Chemistry, University of California, Davis, California 95616

Received: November 23, 1992

We have employed Raman dispersion, FT Raman, and FT-IR spectroscopy to identify a large number of resonance Raman lines of Ni(II) octaethyltetraphenylporphyrin dissolved in CS_2. The Raman depolarization dispersion technique was used to derive the symmetry of the normal modes giving rise to the observed Raman lines. By combining this information and the already available normal coordinates of Ni(II) tetraphenylporphyrin and Ni(II) octaethylporphyrin, many of the Raman-active modes of the macrocycle could be assigned. Some resonance-enhanced Raman lines were found to arise from vibrations of the ethyl and phenyl substituents. They were identified by comparing resonance Raman, FT Raman, and FT infrared spectra of the Ni(II) octaethyltetraphenylporphyrin and its d_{20} isotopomer. All Raman lines normally referred to as core-size markers are found to be significantly shifted to lower frequencies with respect to their positions in Ni(II) octaethylporphyrin, in accordance with earlier findings (Shelnutt et al., *J. Am. Chem. Soc.* **113**, *4077*, 1991). This suggests that the molecule is in a highly nonplanar conformation. This notion is further corroborated by the strong dispersion of the depolarization ratio observed for nearly all A_{1g} and A_{2g} modes of the macrocycle.

Introduction

As has been shown in earlier studies,[1-5] highly substituted metalloporphyrins are generally nonplanar owing to steric crowding of the peripheral substituents (PS) attached to the methine (C_m) and β-carbons (C_β). The macrocycle of the highly symmetric Ni(II) octaethylporphyrin (NiOEP) exhibits two different conformers in solution, one of which is planar and the other nonplanar.[3-5] Molecular mechanics calculations and resonance Raman data have provided evidence that the macrocycle becomes even more nonplanar if phenyl and alkyl groups are attached to both the C_m and C_β atoms, respectively [Ni(II) octaalkyltetraphenylporphyrins (NiOATPP)].[4-6]

Nonplanar porphyrins are thought to play a role in the function of various biological molecules, e.g., in heme proteins,[7] and in the photoreaction center of *Rhodopseudomonas viridis*,[8] methyl-reductase,[9] and vitamin B_{12}.[10] The NiOATPPs should therefore be considered as model substances suited for the investigation of the relationship between porphyrin nonplanarity and function, i.e., the capability to bind a ligand to its central metal atom or to accept/donate an electron in electron-transfer systems.

It is widely recognized that resonance Raman spectroscopy is an excellent tool to study the structural properties of porphyrin systems. For this purpose, however, it is necessary to decompose the rather complex Raman spectra into single lines, which must then be assigned to the normal modes of the molecule. While this has so far been done for the planar molecules NiP, NiTPP, and NiOEP,[11,12] a complete assignment of the Raman lines of the nonplanar NiOATPPs is still in its emergence owing to the lack of knowledge on their normal coordinates and isotopic substitution data.

This paper is dedicated to making preliminary assignments of Raman and infrared lines of Ni(II) octaethyltetraphenylporphyrin (NiOETPP) (Figure 1) by means of various experimental techniques. First, resonance Raman dispersion spectroscopy (RDS)[13] was applied to derive the symmetry of the normal modes giving rise to the lines in the resonance Raman spectra. Second, we used the normal coordinates of NiTPP and NiOEP[11,12] as reference systems for the assignment of the Raman lines to distinct normal modes. Third, in order to identify the contributions of the PS (i.e., phenyl and ethyl), we measured the Fourier transform infrared (FT-IR) and Raman (FT-R) spectra. Finally, the phenyl lines were identified by comparing the corresponding spectra (resonance Raman, FT-R, and FT-IR) of NiOETPP and its isotopomer NiOETPP-d_{20}, in which all the phenyls are perdeuterated. Our results provide a good basis for future work on a normal-coordinate analysis.

Materials and Methods

Preparation of Samples. NiOETPP and its d_{20} isotopomer were prepared as detailed earlier[14,15] and dissolved in CS_2. HPLC-grade CS_2 from Aldrich was purified by silicate chromatography to remove water residuals. The concentration of NiOETPP was determined by measuring the absorption with a 8451A-Hewlett-Packard diode array spectrometer. For the preparation of KBr pellets for the FT-R and FT-IR experiments 1 mg of sample was mixed with about 300 mg of dried fine-grind KBr. The concentration was about 0.3% by weight. The mixture was pressed by standard hydraulic press with a stepwise increase of the pressure to about 8 tons. The same pellet was used for both FT-R and FT-IR spectroscopies, to facilitate direct comparison.

Resonance Raman Spectroscopies. Samples of 1 mM NiOETPP were excited in a 45° backscattering geometry by using an excimer pumped dye laser (Lambda Physik). The pulse energy was 1 mJ at a 200-Hz repetition rate and a pulse length of about

* Authors to whom correspondence should be addressed.
† University of Bremen.
‡ Hong Kong University of Science and Technology.
§ Sandia National Laboratories and University of New Mexico.
∥ University of California.

0022-3654/93/2097-3701$04.00/0

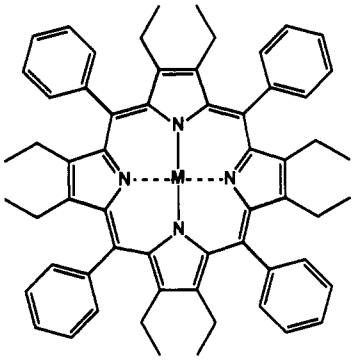

Figure 1. Structure of Ni(II) octaethyltetraphenylporphyrin. For clarity, the hydrogen atoms are omitted from the figure.

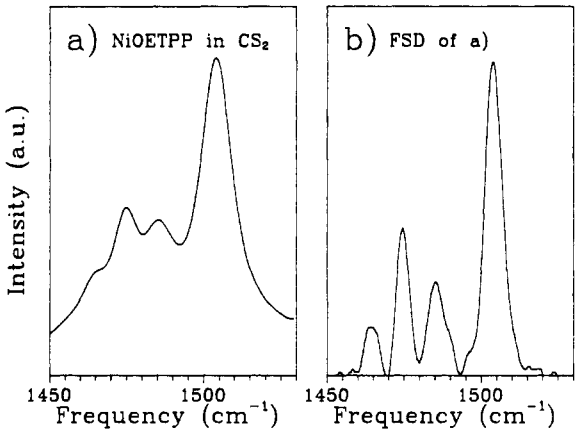

Figure 2. (a) Resonance Raman spectrum of NiOETPP in CS_2 between 1450 and 1530 cm^{-1}. The molecule was excited at 450 nm. (b) Fourier self-deconvolution (FSD) of the spectrum shown in panel a. The mathematical basis of the FSD is given under Materials and Methods.

10 ns. Thus an average laser power of 200 mW was provided. The incident beam was polarized perpendicular to the scattering plane, filtered by two pin holes (stray light suppression), and focused by a cylindrical lens of 40-cm focal length on a spinning quartz cell. The measurements were carried out at room temperature. A polarization analyzer between the sample and the entrance slit enabled us to measure the intensity of the two components perpendicular and parallel to the scattering plane. The scattered light was dispersed by a SPEX triple monochromator 1402 with a spectral resolution of about 5 cm^{-1} and detected by a CCD camera. This system provides 512 channels for data acquisition, thus covering a spectral range of 14 nm. It enabled us to add up a large number of spectra from the same sample to improve the signal-to-noise ratio even at low excitation power. The collected data were stored on an IBM-AT computer for further analyses. A polarization scrambler was used to avoid different transmissions of the spectrometer for different polarizations.

To decompose the complex Raman spectra, we employed the following protocol:

(1) The line frequencies were roughly estimated by inspection of the spectra.

(2) The spectral resolution was improved by utilizing the Fourier self-deconvolution technique (FSD),[16] i.e., the deconvolution of the natural line shape $L(\Omega)$ (Ω: frequency position in the Raman spectrum) from the experimentally observed spectrum $D(\Omega)$, by using the equation:

$$D_{FSD}(\Omega) = FT[A\ FT\{D(\Omega)\}/FT\{L(\Omega)\}] \qquad (1)$$

A is an apodizing function used to avoid side loops in the Fourier transformed spectra and FT denotes the Fourier transform operator.

Figure 2 compares the measured Raman spectrum (panel a) of NiOETPP excited at 450 nm with the corresponding FSD (panel b), thus demonstrating the significantly improved spectral resolution of the latter.

(3) Based on the results emerging from steps 1 and 2, the third step is a first attempt to fit the experimental spectra in a least-squares procedure. To this end, we used the following model function:

$$M(\Omega_i) = \sum_{j=1}^{k} F_j(\Omega_i) + \sum_{l=1}^{m} b_l \Omega_i^l \qquad (2)$$

where Ω_i is the frequency of the ith sampling point, and $F_j(\Omega_i)$ describes the measured band profile and is calculated by convoluting the natural line shape $L(\Omega_i)$ with the spectrometer function which was found semiempirically. The second term is a polynomial function describing the base line. The quality of the fits were judged by the χ^2 function defined by

$$\chi^2 = {}^1/_4 \sum_{i=1}^{s} [(D_i - B_i)/(|D - B|) - (M_i - B_i)/(|M - B|)]^2 \qquad (3)$$

where D_i and M_i are the values of the ith sampling point of the experimental and fitted spectra D and M, respectively. The special normalization chosen in eq 3 is required for step 5 described below. B_i denotes the ith sampling point of the digitized base line.

Next we calculated the probability for finding N Raman lines in the interval δE by use of the equation:

$$P_N = \frac{N!(4\pi)^N \exp(-\chi^2_{min}/2)}{(\delta E)(A_{max})\mathrm{DHM}(\chi^2)} \qquad (4)$$

where A_{max} is the integrated intensity scattered into the interval δE and χ^2_{min} is the minimum of the χ^2 function corresponding to the above preliminary fit to the data. DHM denotes the determinant of the Hessian matrix of χ^2.

To decide on the number of lines in the considered interval, we first fit the spectrum (assuming that N lines are present in the interval δE) and calculated the corresponding χ^2_{min} and P_N by use of eqs 3 and 4. Then we assumed that another line was contributing and calculated the corresponding probability P_{N+1}. To this end, the optimal position of the (N + 1)-th line was obtained by minimization of eq 3. The procedure was finished when P_{N+1} was found to be smaller than P_N. This technique is known as Bayesian spectral analysis (BSA).[17]

(4) We utilized the frequency positions derived from FSD and BSA to derive the final model function $M(\Omega_i)$ for the Raman spectrum.

The polarized Raman scattring intensities $I(\Omega_L)$ parallel and perpendicular to the scattering plane (Ω_L: frequency of the exciting laser beam) of NiOETPP were obtained by applying the above analysis to the Raman spectra measured in 2–3-nm intervals between 420 nm (Ω_L = 23.810 cm^{-1}) and 620 nm (Ω_L = 16.130 cm^{-1}). Thus, the data cover the resonance and preresonance regions of the Q_0, Q_v, and B_0 bands (cf. the optical spectrum in Figure 3).

(5) The quality of a set of self-consistent fits of eq 2 to these Raman spectra was checked by calculating the dispersion of χ^2_{min} with respect to the excitation wavelength. As illustrated in Figure 4a, an imperfect fit gives rise to a χ^2_{min} dispersion, whereas an almost Ω_L-independent χ^2_{min} suggests that the entire fitting procedure yielded satisfactory results (Figure 4b).

In order to illustrate the capability of our deconvolution strategy, Figure 5 shows the highly complex fingerprint region between 1450 and 1530 cm^{-1} measured at 450 and 560 nm (Q_v band) and its decomposition into different Raman lines, the frequencies of which are 1456, 1464, 1475, 1485, 1490, 1499, 1504, and 1509 cm^{-1}.

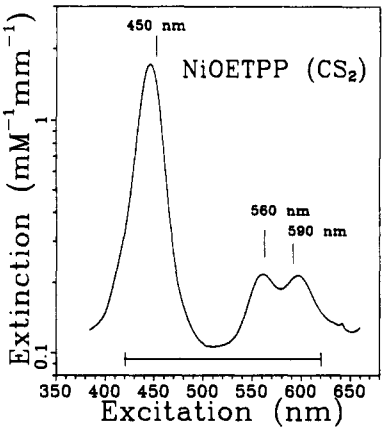

Figure 3. UV–vis spectrum of NiOETPP in CS_2 measured between 350 and 650 nm. The spectral region covered by the resonance Raman data of the polarized excitation profiles (Figures 11 and 12) is marked at the bottom. The numbers above the spectra indicate the wavelengths at which the Raman spectra of NiOETPP (CS_2) shown in Figure 6 are observed.

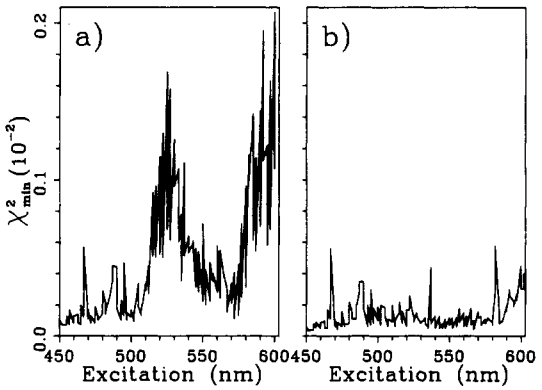

Figure 4. χ^2_{min} dispersion for an imperfect (a) and a satisfactory (b) set of fits to the high-frequency (900–1700-cm^{-1}) Raman spectra measured at wavelengths between 450 and 620 nm as described under Materials and Methods.

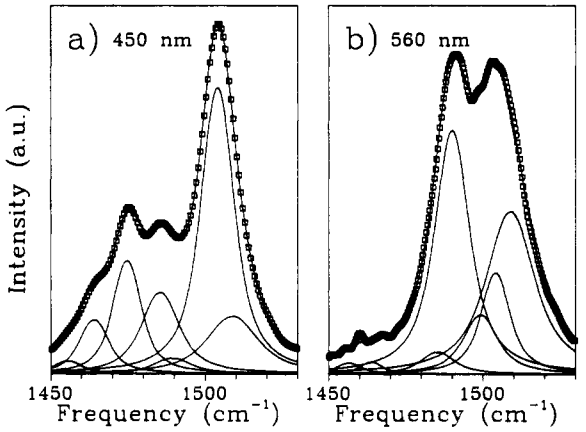

Figure 5. Raman lines of NiOETPP in CS_2 (solid lines) contributing to the complex spectra between 1450 and 1530 cm^{-1} (□—□) measured at 450 and 560 nm. The decomposition was achieved by using the analytical techniques described under Materials and Methods.

Finally, the derived intensities of the Raman lines were normalized to the isolated line of the CS_2 solvent at 652 cm^{-1}. The depolarization ratio, ρ, was then calculated as

$$\rho(\Omega_L) = I_{\parallel}(\Omega_L)/I_{\perp}(\Omega_L) \qquad (5)$$

The above protocol provides the Raman lines in the high-frequency region of the spectrum between 900 and 1700 cm^{-1}. To identify some of the low-frequency modes, we also measured

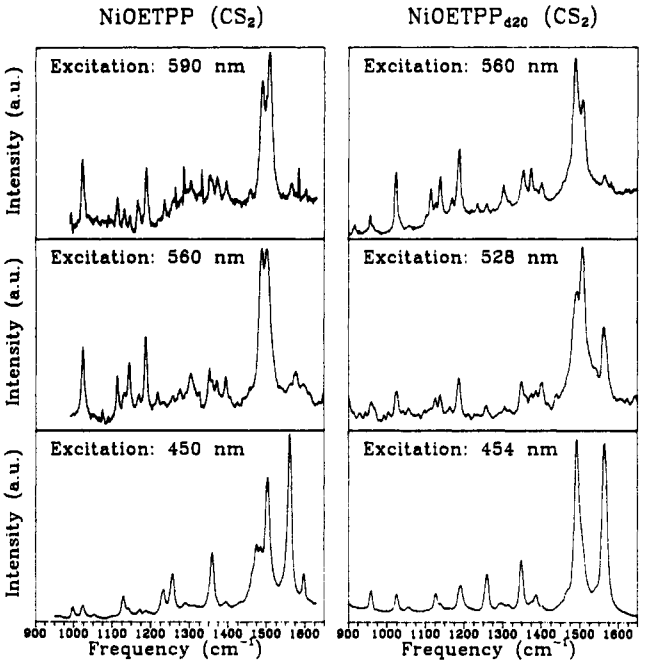

Figure 6. High-frequency resonance Raman spectra (900–1700 cm^{-1}) of NiOETPP and its d_{20} isotopomer in CS_2 measured at the indicated wavelengths as described under Materials and Methods. The spectra in the upper and middle panels are dominated by Raman lines arising from Q-state scattering. The lower panels exhibit a typical B-state spectra.

the polarized spectra between 200 and 900 cm^{-1} at 457-nm excitation wavelength with an argon ion laser (Spectra Physics). The experimental setup is described elsewhere.[18a]

In order to identify the NiOETPP Raman lines resulting from phenyl vibrations, we measured some polarized Raman spectra of the NiOETPP-d_{20} isotopomer with the excimer pumped dye laser (900–1700 cm^{-1}) and the argon ion laser (150–900 cm^{-1}).

FT-IR and FT-R Spectroscopies. FT-R and FT-IR spectra were obtained with a Bruker IFS 66/FRA 106 spectrometer. In FT-R measurements, the sample was irradiated by 200 mW from a CW Nd:YAG laser fundamental (1064 nm) in a 180° scattering geometry. Approximately 2000 scans were collected for each sample to obtain an appropriate signal-to-noise ratio. A Ge detector cooled with liquid N_2 was used to detect the FT-R signals.

For FT-IR spectra, the IFS 66 mode of the above Bruker spectrometer was used. KBr splitter and KBr windows covered a DTGS detector which operated at room temperature for the detection of IR signals.

The resolution of both FT-IR and FT-R were set at 4 cm^{-1} for the FT-IR spectra; typically 50 scans were collected to increase the signal-to-noise ratio. For the FT-R spectra, 1000 scans were averaged. All experiments were repeated at least twice to assure the reproducibility of weak peaks.

Results and Discussion

Some resonance Raman spectra of NiOETPP and its d_{20} isotopomer are shown in Figures 6 and 7. Figure 6 displays the high-frequency region between 900 and 1700 cm^{-1} measured with an excimer pumped dye laser. The upper and middle panels herein exhibit spectra which are governed by Q_0- and Q_v-band excitation, respectively, whereas the spectra shown in the lower panels are measured in the B-band region (cf. Figure 3). Figure 7 depicts the low-frequency region between 150 and 900 cm^{-1} of the above samples which were measured with the 454- and 457-nm lines of an argon ion laser.

The corresponding FT-R and FT-IR spectra of NiOETPP and its d_{20} isotopomer were recorded between 400 and 1700 cm^{-1} and are shown in Figures 8 (900–1700 cm^{-1}) and 9 (400–900 cm^{-1}). Additionally, we measured the FT-IR spectra between 2200 and

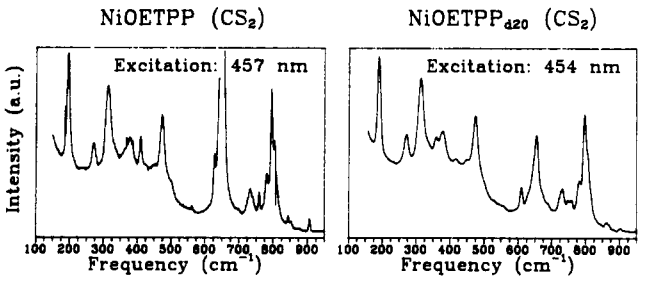

Figure 7. Low-frequency spectra (150–950 cm^{-1}) of NiOETPP and its d_{20} isotopomer in CS_2 measured at 457 nm (454 nm) as described under Materials and Methods.

3400 cm^{-1} in order to obtain the frequencies of the CH stretching vibrations of the phenyl and ethyl substituents. These data are shown in Figure 10. They clearly show the absence of CH vibrations of the phenyls in the spectrum of the d_{20} isotopomer, thus demonstrating the high purity of the sample employed.

Most of the lines observed from the above spectra were assigned to distinct normal modes of the macrocycle and its PS by the following strategy.

Determination of the Normal-Mode Symmetry in the Undistorted D_{4h} Symmetry. In order to determine the symmetry of the Raman-active porphyrin modes, we measured the polarized resonance excitation profiles (REPs) by utilizing the methods described. From these we calculated the depolarization ratio as a function of the excitation wavelength. It turns out that the major part of the Raman lines exhibit a drastic dispersion of their depolarization ratios (DPD). This clearly suggests that the symmetry of the macrocycle is lowered from its ideal D_{4h} symmetry, which is most probably due to out-of-plane distortions giving rise to the saddle structure of NiOETPP.[4,5,18a]

Two different types of Raman lines can easily be discriminated by the above dispersion studies. The first one exhibits a significant DPD. These lines are nearly polarized in the Soret band region (ρ = 0.125–0.25) and are highly anomalously polarized between their Q_0 and Q_v resonance positions (cf. Figure 11). This feature clearly suggests that A_{1g} and A_{2g} contributions are admixed into the scattering tensor.[19-21] It further indicates that the symmetry of the macrocycle is at least lowered to C_4 or S_4, in which A_{1g} and A_{2g} collapse into one common representation A.[6]

The corresponding D_{4h} symmetry species of these Raman lines can be derived from the maximal ρ-value of their DPDs. The 1359-cm^{-1} line, for instance, exhibits a ρ_{max} of 1.5 (Figure 11), whereas the ρ_{max} value of the 1490-cm^{-1} line has been found to be larger than 10 (Figure 11). This suggests that A_{1g} contributions are dominant in the Raman tensor of the former line, while the latter one is mainly determined by A_{2g} contributions. Moreover, the 1359-cm^{-1} line is predominantly enhanced in the B-band region, suggesting that A_{1g}-type Franck–Condon coupling is operative.[23] In contrast, the 1490-cm^{-1} line is mainly excited at the Q_0 and Q_1 resonance positions, and its REP suggests constructive interference between Q_0 and Q_v. This is indicative of strong A_{2g}-type Herzberg–Teller coupling.[27] Consequently, we attributed the first line to an A_{1g}-type vibration (ν_4) and the latter one to an A_{2g}-type mode (ν_{19}) in the undistorted D_{4h} symmetry. The assignment of the remaining A-type modes was made in a similar way.

The second type of Raman lines is nearly depolarized (ρ = 0.75) at all excitation wavelengths (Figure 12). Only a few of them exhibit some DPD in the Q-band region (for instance, 1499 cm^{-1}, Figure 12). They can be attributed to the symmetry B in C_4 or S_4. The depolarization ratio cannot be used to discriminate between modes whose symmetry is B_{1g} and B_{2g} in ideal D_{4h}. Comparison of the REPs of unambiguously assigned B_{1g} and B_{2g} modes of ferrocytochrome c,[21] NiOEP,[13] and NiP,[22] shows, however, that B_{1g}-type modes exhibit larger intensities in the Q_0 region than at their Q_v resonance position. The B_{2g} modes

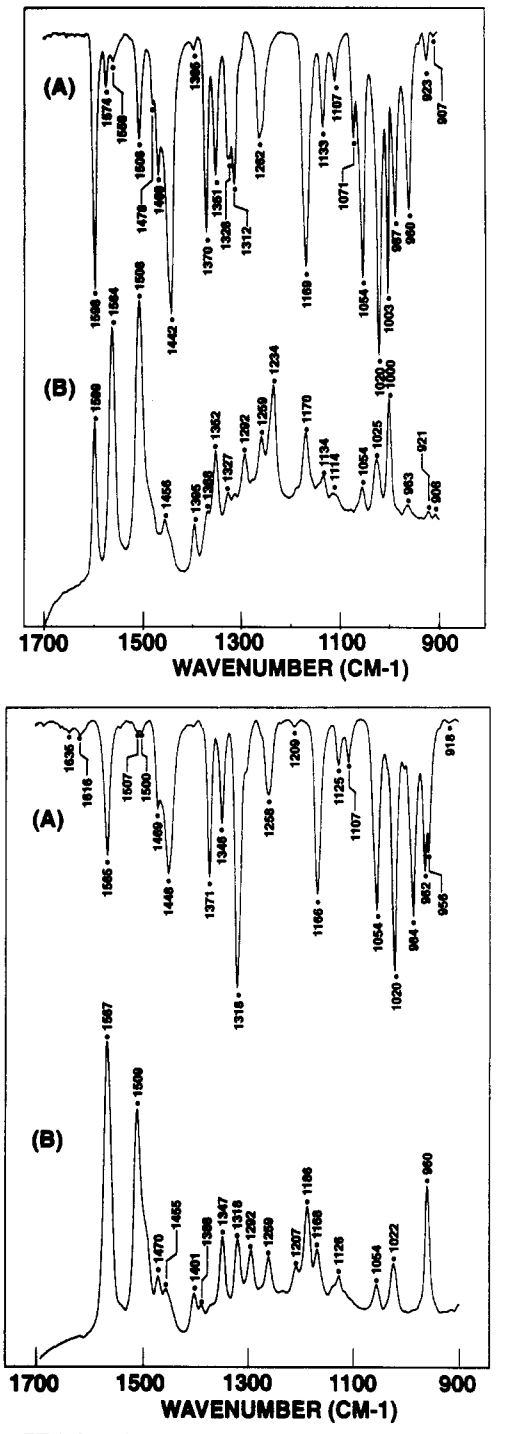

Figure 8. FT infrared (A) and FT Raman (B) spectra of NiOETPP (upper panel) and its d_{20} isotopomer (lower panel) in KBr pellets recorded between 900 and 1700 cm^{-1}. The data were observed as described under Materials and Methods.

were found to behave oppositely. Assuming that this also holds for NiOETPP, we utilized the REPs of the B-type lines to discriminate between modes whose unperturbed symmetry is B_{1g} or B_{2g}. Consequently, the REPs of the 1509- and 1499-cm^{-1} lines shown in Figure 12 are interpreted as indicative of normal modes of B_{1g} and B_{2g} symmetry, respectively.

Identification of Raman Lines. The normal coordinates of NiTPP and NiOEP[11,12] were utilized to identify the Raman lines corresponding to the normal modes. In a first approximation the latter are not expected to be responsive to the ethyl substitution at the C_β of NiTPP or to phenyl substitution at the C_m of NiOEP. Hence we assumed the ethyl vibrations to have similar frequencies in NiOEP and NiOETPP, while the phenyl vibrations should appear at similar positions in NiTPP and NiOETPP. Even though

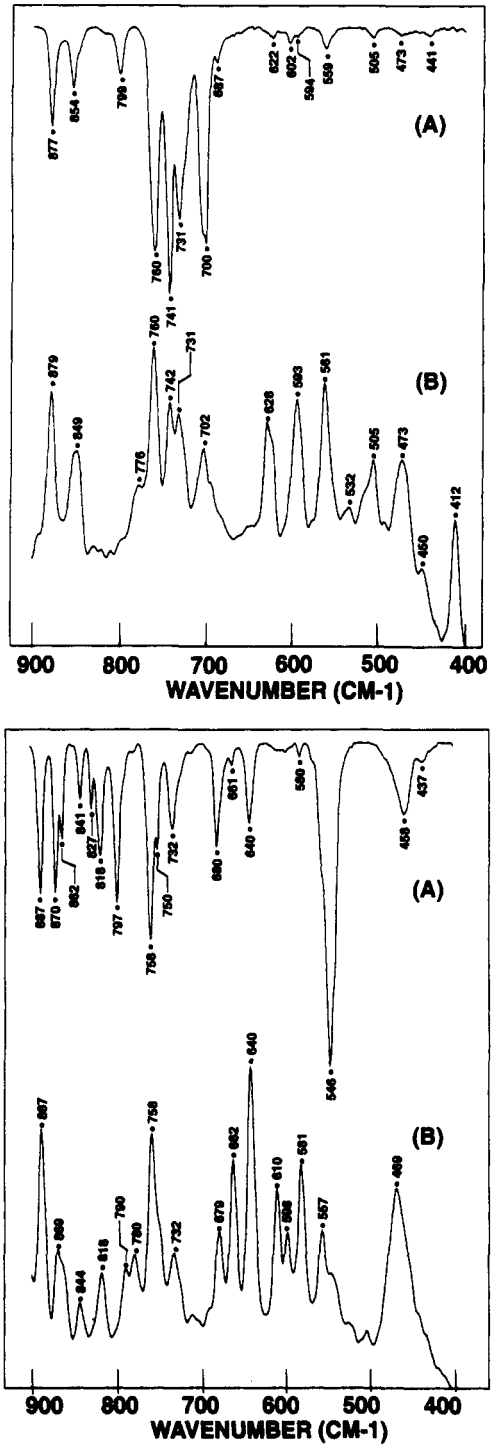

Figure 9. FT infrared (A) and FT Raman (B) spectra of NiOETPP (upper panel) and its d_{20} isotopomer (lower panel) in KBr pellets recorded between 400 and 900 cm^{-1}. The data were observed as described under Materials and Methods.

this strategy is not fully applicable, it facilitated the assignment of a large number of Raman lines.

The recently performed normal-coordinate analyses of NiOEP and NiTPP[11,12] also provide the frequencies and compositions of the ethyl and phenyl modes of these molecules, respectively. By combining these results with the information obtained from the comparison of resonance Raman, FT-R, and FT-IR spectra of NiOETPP and its d_{20} isotopomer, we identified some of the PS lines in these complex spectra.

The above procedure enabled us to attribute several vibrational bands appearing in the resonance Raman, FT-R, and FT-IR spectra to distinct macrocycle and PS modes as given in Table I.

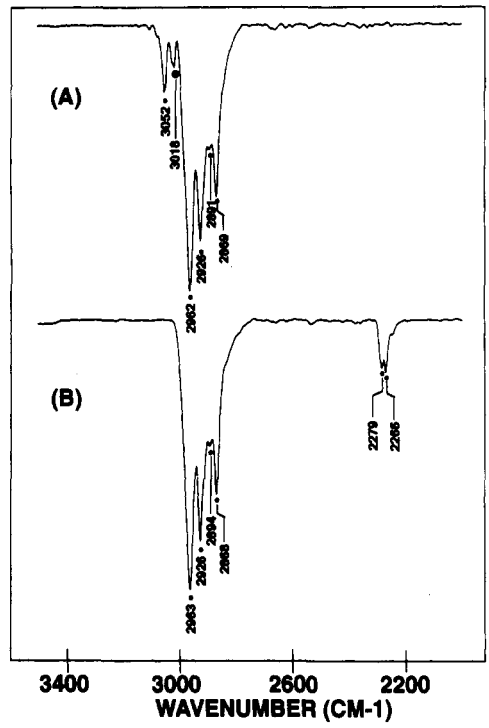

Figure 10. FT infrared spectra of NiOETPP (A) and its d_{20} isotopomer (B) in KBr pellets recorded in the high-frequency region between 2200 and 3400 cm^{-1}. The data were observed as described under Materials and Methods.

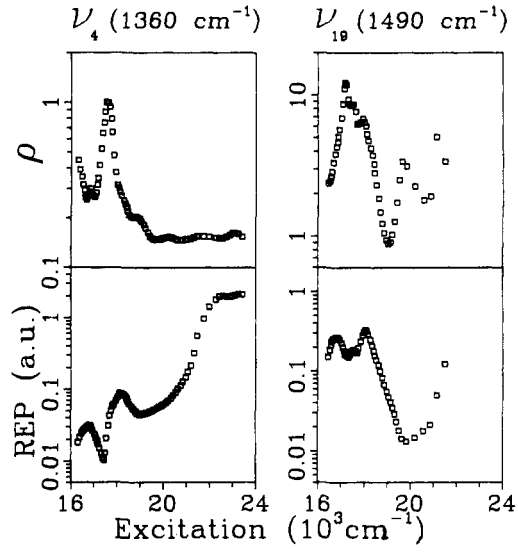

Figure 11. DPDs and REPs of the Raman lines at 1360 and 1490 cm^{-1}. The data were obtained from the Raman spectra as described under Materials and Methods.

Raman-Active Modes of the Porphyrin Macrocycle. We are now able to characterize the resonance Raman spectra shown in Figures 6 and 7. The spectra shown in the upper and middle panels of Figure 6 mainly result from B_{1g} and B_{2g} modes which are resonance enhanced at the Q_0 and Q_v positions owing to Jahn–Teller coupling within the Q states and Herzberg–Teller coupling between the Q and B[21-24] states. The antisymmetric A_{2g} modes are exclusively enhanced by Herzberg–Teller coupling between Q and B. The spectra in the lower panel display Raman lines mainly arising from A_{1g} modes which are resonance enhanced by Franck–Condon transitions into the B states.[23] Nevertheless, it should be noted that lines from asymmetric modes appear in the B band and lines from symmetric modes show up in the resonance region of the Q band, but their intensities are comparatively weak (cf. Table I and Figure 6).

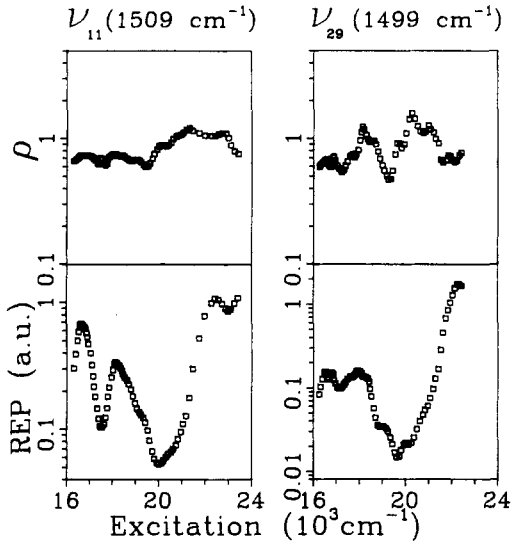

Figure 12. DPDs and REPs of the Raman lines at 1499 and 1509 cm^{-1}. The data were obtained from the Raman spectra as described under Materials and Methods.

The Q-band spectra in Figure 5 are dominated by the Raman lines assigned to ν_{19} (1490 cm^{-1}, A_{2g}) and ν_{11} (1509 cm^{-1}, B_{1g}), which are mainly provided by C_α–C_m and C_β–C_β vibrations, respectively.[11,12] Some lines exhibiting intermediate intensities show up in the region between 1000 and 1200 cm^{-1}. They were attributed to ν_{14} (1169 cm^{-1}, B_{1g}), ν_{30} (1145 cm^{-1}, B_{2g}), ν_{22} (1188 cm^{-1}, A_{2g}), and ν_{23} (1114 cm^{-1}, A_{2g}). In contrast to ν_{11} and ν_{19}, which are rather localized modes, their modes are determined by a combination of various stretching and bending motions, for instance, $\nu(C_\alpha N)$, $\nu(C_\alpha C_\beta)$, $\nu(C_\beta C_1)$ (C_1 is an ethyl carbon), and $\delta(C_\alpha C_\beta C_\beta)$.[11,112] This indicates that the excited electronic states $Q_{x,y}$ and $B_{x,y}$ and the electronic ground state are displaced with respect to each other along normal coordinates which mainly involve the C_α–C_m and C_β–C_β bonds.[24,25]

Two other Raman lines which, owing to their polarization properties, should be assigned to A_{2g} vibrations are observed at 1372 and 1352 cm^{-1}. Only one of these lines, however, can be assigned to an antisymmetric macrocycle mode (ν_{20}), because the ν_{21} mode is expected to be downshifted to lower frequencies.[11] The other one may be attributed to a CH_2 wagging mode. Because the 1352-cm^{-1} line exhibits a slightly stronger maximal intensity at the resonance positions, it is tentatively attributed to ν_{20}.

The B-band spectra in the lower panels are dominated by the Raman lines arising from ν_2 (1563 cm^{-1}, A_{1g}) and ν_3 (1504 cm^{-1}, A_{1g}). The Raman line of the ν_4 mode, which is the most intense one in the B-band spectra of heme proteins [Fe(II) protoporphyrin IX and heme c][21,23,26] and NiOEP,[13] exhibits only an intermediate intensity comparable with that of ν_1 (1235 cm^{-1}, A_{1g}) and ν_5 (1131 cm^{-1}, A_{1g}). This may again be explained by considering differences in the normal-mode composition. Both ν_2 and ν_3 get major contributions from $\nu(C_\alpha C_m)$ and $\nu(C_\beta C_\beta)$, to which phenyl contributions are admixed.[12] The ν_4 mode, however, has been shown to be governed by pyrrole half-ring vibration which, to a large extent, consists of $\nu(C_\alpha C_\beta)$ and $\nu(C_\alpha N)$.[11,12] Thus, the intensity patterns of the A_{1g} lines also indicate that the B state is displaced with respect to the ground state along those coordinates depending on the C_α–C_m and C_β–C_β bonds.[25] A thorough analysis of the resonance excitation profiles and the depolarization ratio dispersion of the above Raman lines, however, is required to get more details on the coupling mechanism that determines their intensities. These investigations are currently underway.

The low-frequency region of the resonance Raman spectrum is determined by the lines resulting from the A_{1g} modes ν_7 (733 cm^{-1}), ν_8 (322 cm^{-1}), and ν_9 (275 cm^{-1}). The comparatively strong lines at 453 and 195 cm^{-1} most probably result from phenyl vibrations which are discussed below in more detail. The polarized line at 314 cm^{-1} is tentatively attributed to the out-of-plane vibration γ_6 (A_{2u}).

As proved by a considerably large number of experimental data, the frequencies of the macrocycle modes ν_2, ν_3, ν_4 (all A_{1g}), ν_{10}, ν_{11} (B_{1g}), and ν_{21} (A_{2g}) are responsive to changes of the porphyrin core size and have been designated as core-size marker lines.[23] As has been shown in earlier papers,[4,5] the core-size dependence of some of the marker lines (ν_2, ν_3, ν_4) is different for a series of planar porphyrins from that for a series of progressively more nonplanar porphyrins. The linear relation between frequency and core size exhibits a negative slope in the former series and a positive slope in the latter one. One observes a linear relationship in both planar and nonplanar porphyrins, with a negative slope between the frequencies of the above lines and the $C_\alpha NC_\alpha$ angle of the pyrroles.

Increasing porphyrin nonplanarity is expected to cause a downshift of the core-size marker lines.[4,5] Our results on NiOETPP show that indeed the frequencies of the marker lines ν_2, ν_3, ν_4, ν_{11}, and ν_{19} are significantly lower with respect to planar NiOEP (cf. Table II). This is true in particular for ν_{19}, which shifts from 1603 cm^{-1} in NiOEP down to 1490 cm^{-1} in NiOETPP.

Deuteration of the phenyls lowers the frequencies of some macrocycle A_{1g} Raman lines above 900 cm^{-1} (i.e., ν_3, ν_4, ν_1, and ν_5; cf. Table I). Corresponding frequency shifts of the identified B_{1g}, B_{2g}, and A_{2g} lines are smaller. This indicates that the A_{1g} modes in particular mix with internal phenyl modes.

Ethyl and Phenyl Modes. Even though neither the ethyls nor the phenyls contribute to the π-electron system of the macrocycle, some of their modes are resonance enhanced in the Q- and B-band region. As shown in a previous study,[13] the A_1- and B_1-type C_1–C_2 ethyl vibrations of NiOEP show comparatively strong intensities in the Q-band region owing to large contributions from Franck–Condon and Jahn–Teller coupling in the Q state and Herzberg–Teller coupling between Q and B. In this study we found Raman-active ethyl modes at 1456 cm^{-1} (CH_2 scis), 1352 cm^{-1} (CH_2 wag), 1312 cm^{-1} (CH_2 wag), 1259 cm^{-1} (CH_2 twist), and 1024 cm^{-1} (C_1–C_2), which show up in the Raman spectra measured in the Q- and B-band region. To give an example, Figure 13 displays the DPDs and REPs of the phenyl mode ϕ_4 at 1599 cm^{-1} and the $\nu(C_1C_2)$ ethyl mode at 1025 cm^{-1}. While the DPD of the 1456-cm^{-1} line indicates a B_1 symmetry, the polarization dispersion of other PS lines shows that A_1, B_1, B_2, and A_2 contributions are admixed to the Raman tensor.[6]

Some phenyl lines could also be identified in the Raman spectra measured in the B-band region (cf. Table I). The lines at 1599 cm^{-1} (ϕ_4), 1485 cm^{-1} (probably ϕ_5), 1475 cm^{-1} ($\phi_{5''}$), 998 cm^{-1} (ϕ_8), and 195 cm^{-1} (ϕ_{10}) exhibit intensities similar to some lines of the macrocycle vibrations. All these lines, with the exception of ϕ_{10}, are downshifted in the deuterated spectra.

The mechanism by which the PS lines become resonance enhanced in the B- and Q-band region is yet unresolved. We believe that this is due to (vibrational) interactions with the nearby macrocycle modes of the same symmetry. This interpretation is supported by the observation that the DPDs of ethyl and phenyl modes parallel those of the macrocycle vibrations. Additional supporting evidence for this interpretation is that PS modes show sensitivity to the isotope labeling on the macrocycle or the macrocycle modes show sensitivity to isotope labeling on the PS.

Summary

By measuring the polarized Raman spectra of NiOETPP at ca. 100 different excitation wavelengths between 420 and 620 nm, we have identified a large number of Raman lines resulting from normal vibrations of the macrocycle and its peripheral substituents. The symmetry of these modes was derived from their depolarization ratio dispersion and resonance excitation profiles. The assignment of the Raman lines to distinct normal

TABLE I: Observed Raman and IR Frequencies for Ni^{II}OETPP and Ni^{II}OETPP-d_{20}[a]

NiOETPP				NiOETPP-d_{20}				
FT-R[b]	RR (B)[c]	RR (Q)[c]	FT-IR[b]	FT-R[b]	RR (B)[c]	RR (Q)[c]	FT-IR[b]	assignment[d]
3056	–	–	3052	2287	–	–	2279	$\nu(CH)_{Ph}$
3012	–	–	3018	2264	–	–	2266	$\nu(CH)_{Ph}$
–	–	–	2962	–	–	–	2962	$\nu(CH)_{Et}$
2926	–	–	2926	2927	–	–	2926	$\nu(CH)_{Et}$
–	–	–	2891	–	–	–	2894	$\nu(CH)_{Et}$
2866	–	–	2869	2868	–	–	2868	$\nu(CH)_{Et}$
1599	1599	1599	1598	1567	1567	1567	1565	$\phi_4(A_1)$
–	1573 (w)	1574 (w)	1574	–	–	–	–	$\phi_{4'}(A_1)$
1564	1563	1563	1559	1567 (o)	1564	1564	1565	$\nu_2(A_1)$
1508	1509	1509	1506 (o)	1509	1507	1507	1507	$\nu_{11}(B_1)$
1508 (o)	1504	1504	1504 (o)	–	1492	1492	–	$\nu_3(A_1)$
1508 (o)	–	–	1506 (o)	1388	1386	1386	1390 (w)	$\phi_{5'}$
–	1499	1499	–	–	–	–	–	$\nu_{28}(B_2)$
–	1490	1490	–	–	–	1492	–	$\nu_{19}(A_2)$
–	1485	1485	–	–	–	–	–	$\phi_5(A_1/A_2)$
–	1475	1475	1478 (w)	–	–	–	–	$\phi_{5'}(A_1/A_2)$
–	1464	–	1469	1470	1468	–	1469	Et(deform.)
1456	1456	1456	1456 (o)	1455	–	–	1455 (o)	Et(deform.)
–	–	–	1442	–	–	1438	1448	Et(deform.)
1395	1395	1395	1395 (w)	1401	1403	1403	1401	$\nu_{29}(B_2)$
–	1372	1372	–	–	–	1375	–	(A_2)
1368	–	–	1370	–	–	–	1371	Et(deform.)
–	1359	1359	–	–	1348	1348	–	$\nu_4(A_1)$
–	1352	1352	–	–	–	1355	–	$\nu_{20}(A_2)$
1352 (o)	–	–	1351	1347	–	–	1346	Et(deform.)
1327	–	–	1326	887	–	–	887	$\delta(CH)_{Ph}$
1312	–	–	1312	1318	–	–	1318	Et(deform.)
–	–	1309	–	–	1304	1304	–	(A_2)
1292	1292 (w)	1292 (w)	–	1292	1293 (w)	–	1292 (sh)	$\nu_{12}(B_1)$
1259	1259	1259	1262	1259	1258	1258	1258	Et(A_1)
–	–	–	–	1207	–	–	1209	
1234	1235	1235	–	1186	1188	1188	–	$\nu_1(A_1)$
–	1188	1188	–	–	1188	1188	–	$\nu_{22}(A_2)$
1170	1169	1169	1169	1168	–	1171	1166	$\nu_{14}(B_1)$
–	1145	1145	–	–	1140	1140	–	$\nu_{30}(B_2)$
1134	1132	1132 (w)	1133	1126	1127	1127	1125	$\nu_5(A_1)$
1114	1114	1114	–	–	–	1115	–	$\nu_{23}(A_2)$
–	–	–	1107	–	–	1104	1107	(B_1/B_2)
–	–	–	1071	–	–	–	827	
1054	1054	1053	1054	1054	1055	1055	1054	(A_1)
1025	1024	1024	1020	1022	1025	1025	1020	$\nu(C_1C_2)(A_1/B_1)$
1000	1000	1000	1003	960	959	959	962	$\phi_8(A_1)_{Ph}$
–	–	–	987	–	–	–	984	
963	964	960	960	960 (o)	959 (o)	959 (o)	956	
921	–	–	923	750 (sh)	–	–	750	$\pi(CH)_{Ph}$
–	–	–	–	–	–	916	918 (w)	(B_1/B_2)
908	907	907	907	900	900	900	–	(A_1)
879	–	–	877	869	867	867	870	
849	844	–	854	844	–	–	841	$\nu_6(A_1)$
–	–	–	–	818	–	–	818	
776	–	–	799	780	–	–	797	$\delta(CH_2$ rock)
760	760	–	760	758	–	–	758	$\nu_{15}(B_1)$
742	–	–	741	679	–	–	680	$\pi(CH)_{Ph}$
731	733	–	731	732	730	–	732	$\nu_7(A_1)$
702	–	–	700	546 (sh)	–	–	546	$\pi(CH)_{Ph}$
–	–	–	–	662	–	–	661	
–	–	–	–	640	–	–	640	
687 (sh)	–	–	687	–	–	–	–	
628	–	–	622	610	608	–	–	
–	–	–	602	–	–	–	–	
–	–	–	–	598	–	–	–	
593	–	–	594 (w)	581	–	–	580	
561	–	–	559	557	–	–	551 (sh)	
505	–	–	505	458 (sh)	–	–	458	
473	477	–	473	469	473	–	469 (sh)	(A_1)
450	453	–	441	–	447	–	437	(A_1)
412	412	–	–	358	358	–	–	(A_1)
384	382	–	–	382	378	–	–	$\nu_8(A_1)$
311	314	–	–	310	312	–	–	
270	275	–	–	251	270	–	–	$\nu_9(A_1)$
238	–	–	–	234	–	–	–	
195	194	–	–	190	190	–	–	$\phi_{10}(A_1)$

Footnotes to TABLE I.

[a] A dash (-) in the table indicates that no corresponding band was observed. w: weak band in the spectra; REP and DPD are not accurate enough to determine the symmetry of the line. o: overlap with another band at same/similar position. sh: shoulder on a strong band. Uncertainty of the line position >2 cm^{-1}. [b] Spectra taken from KBr pellet with ≈0.3% sample concentration by weight. FT-R: bands observed in the near-infrared-excited (1064-nm) fourier transform Raman spectra. FT-IR: bands obsereved in the Fourier transformed infrared absorption spectra. See text for details. [c] Spectra taken in CS_2 solution. RR (B): bands observed with excitations near Soret (B) absorption. RR (Q): bands observed with excitations near Q_0 and Q_v absorption. [d] Mode numbering follows that proposed by Li et al.[11] for NiOEP and NiTPP. Listed numbers are for Raman-active modes only; IR lines listed in the same row have similar local coordinate character as corresponding Raman lines, but belong to different symmetry species. Symbols in parentheses are the symmetry species as indicated by REP and DPD; see text for detailed discussion. ν: stretching character. δ: bending character. π: out of plane bending (phenyl) bending character. Subscript Ph: phenyl mode. Subscript Et: ethyl mode.

TABLE II: Core-Size-Sensitive Marker Modes of NiOEP and NiOETPP

assignment	NiOETPP	NiOEP
ν_2	1563	1603
ν_3	1504	1520
ν_4	1359	1383
ν_{10}	(1540)[a]	1655
ν_{11}	1509	1577
ν_{19}	1490	1602

[a] Estimated frequency.

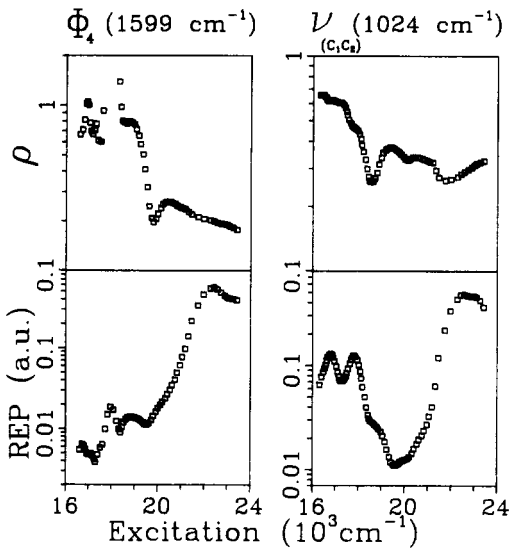

Figure 13. DPDs and REPs of the Raman lines at 1599 and 1024 cm^{-1} arising from vibrations of the phenyl (ϕ_4) and ethyl substituents, respectively. The data were obtained from the Raman spectra as described under Materials and Methods.

modes was then made on the basis of the recently obtained normal coordinates of NiTPP and NiOEP.[11,12] FT Raman and FT infrared spectra were recorded to identify contributions from the peripheral substituents. Discrimination between ethyl and phenyl modes was achieved by comparing the resonance Raman, FT Raman, and FT infrared spectra of NiOETPP with those of its d_{20} isotopomer, in which all phenyls are deuterated.

The frequencies of the "core-size markers" ν_2, ν_3, ν_4, ν_{11}, and ν_{19} are significantly downshifted with respect to their position in NiOEP.[11] This confirms that NiOETPP is in a nonplanar conformation solution.[4,5] This notion is corroborated by the strong dispersion of the depolarization ratio of all A_{1g} and A_{2g} lines in the high-frequency region between 900 and 1700 cm^{-1}.

Acknowledgment. We gratefully acknowledge that the work at Sandia National Laboratories was supported by a grant from the U.S. Department of Energy to J.A.S. (DE-AC04-76DP00789). L.D.S. acknowledges an Associated Western Universities, Inc., graduate fellowship. A.S. is the recepient of a University of Bremen fellowship. Research at U.C. Davis was supported by a grant from the National Institutes of Health to K.M.S. (HL-22252). C.J.M. acknowledges a Fulbright Travel Scholarship and an Associated Western Universities Postdoctoral Fellowship. X.L. acknowledges the partial financial support of this work by an RGC grant (HKUST 10/91) administrated by UPGC, Hong Kong.

References and Notes

(1) Cullen, D. L.; Meyer, E. F., Jr. *J. Am. Chem. Soc.* **1976**, *96*, 2095.
(2) Cernuszewicz, R. S.; Li, X.-Y.; Spiro, T. G. *J. Am. Chem. Soc.* **1989**, *111*, 7024.
(3) Alden, R. G.; Crawford, B. A.; Doolen, R.; Ondrias, M. R.; Shelnutt, J. A. *J. Am. Chem. Soc.* **1989**, *111*, 2070.
(4) Shelnutt, J. A.; Medforth, C. J.; Berber, M. D.; Barkigia, K. M.; Smith, K. M. *J. Am. Chem. Soc.* **1991**, *113*, 4077.
(5) Shelnutt, J. A.; Hobbs, J. D.; Majumder, S. A.; Sparks, L. D.; Medforth, C. T.; Senge, M. O.; Smith, K. M.; Miura, M.; Quirke, J. M. E. *J. Raman Spectrosc.* **1992**, *23*, 523.
(6) Stichternath, A.; Schweitzer-Stenner, R.; Dreybrodt, W.; Medforth, C. J.; Smith, K. M. *Proceedings of the XIII International Conference on Raman Spectroscopy*; Kiefer, W., Cardona, M., Schaak, G., Schneider, F. W., Schrötter, H. W., Eds. Wiley: Chichester, 1992; pp 132–133. (b) Stichternath, A.; Schweitzer-Stenner, R.; Dreybrodt, W.; Medforth, C. J.; Smith, K. M. Manuscript in preparation.
(7) Baldwin, J. L.; Chotia, C. *J. Mol. Biol.* **1979**, *129*, 175.
(8) Deisenhofer, J.; Epp, O.; Miki, K.; Huber, R.; Michel, H. *Nature* **1985**, *318*, 618.
(9) Furenlid, L. R.; Renner, M. W.; Smith, K. M.; Fajer, J. *J. Am. Chem. Soc.* **1990**, *112*, 1634.
(10) Geno, M. K.; Halpern, J. *J. Am. Chem. Soc.* **1986**, *109*, 1238.
(11) Li, X.-Y.; Czernuszewicz, R. S.; Kincaid, J. R.; Stein, P.; Spiro, T. G. *J. Phys. Chem.* **1990**, *94*, 31.
(12) Li, X.-Y.; Cernuszewwicz, R. S.; Kincaid, J. R.; Stein, P.; Spiro, T. G. *J. Phys. Chem.* **1990**, *94*, 47.
(13) Bobinger, U.; Schweitzer-Stenner, R.; Dreybrodt, W. *J. Phys. Chem.* **1991**, *95*, 7625.
(14) Medforth, C. J.; Berber, M. D.; Smith, K. M.; Shelnutt, J. A. *Tetrahedron Lett.* **1990**, *31*, 3719.
(15) Medforth, C. J.; Smith, K. M. *Tetrahedron Lett.* **1990**, *31*, 5583.
(16) Kapinene, J. K.; Moffat, D. J.; Mantsch, H. H.; Cameron, D. G. *Appl. Spectrosc.* **1981**, *35*, 271.
(17) Sivia, D. S.; Carlile, C. J. *J. Chem. Phys.* **1992**, *96*, 170.
(18) (a) El Naggar, S.; Dreybrodt, W.; Schweitzer-Stenner, R. *Eur. Biophys. J.* **1985**, *13*, 43. (b) Barkigia, K. M.; Fajer, J.; Medforth, C. J.; Smith, K. M. Submitted to *J. Am. Chem. Soc.*
(19) Zgierski, M. Z.; Pawlikowski, M. *Chem. Phys.* **1982**, *65*, 335.
(20) Bobinger, U.; Schweitzer-Stenner, R.; Dreybrodt, W. *J. Raman Spectrosc.* **1989**, *20*, 191.
(21) Schweitzer-Stenner, R.; Bobinger, U.; Dreybrodt, W. *J. Raman Spectrosc.* **1991**, *22*, 65.
(22) (a) Unger, E.; Bobinger, U.; Schweitzer-Stenner, R.; Dreybrodt, W. *Proceedings of the XIII International Conference on Raman Spectroscopy*; Kiefer, W., Cardona, M., Schaak, G., Schneider, F. W., Schrötter, H. W., Eds.; Wiley: Chichester, 1992; pp 144–145. (b) Unger, E.; Bobinger, U.; Schweitzer-Stenner, R.; Dreybrodt, W. Manuscript in preparation.
(23) Spiro, T. G.; Li, X.-Y. In *Biological Applications of Raman Spectroscopy*; Spiro, T. G., Ed.; Wiley: New York, 1988; pp 1–38.
(24) Shelnutt, J. A.; Cheung, L. D.; Chang, R. C. C.; Yu, N. T.; Felton, R. H. *J. Chem. Phys.* **1977**, *66*, 3387.
(25) Tsuboi, M.; Hirakawa, A. Y. *J. Raman Spectrosc.* **1976**, *5*, 75.
(26) Stallard, B.; Callis, P. R.; Champion, P. M.; Albrecht, A. C. *J. Chem. Phys.* **1984**, *80*, 70.
(27) Zgierski, M. Z.; Shelnutt, J. A.; Pawlikowski, M. *Chem. Phys. Lett.* **1979**, *68*, 262.